Transition Metal Chemistry (2006) 31:920–929
DOI 10.1007/s11243-006-0087-0
© Springer 2006

Synthesis, characterization, catalytic, electrochemical and thermal properties of tetradentate Schiff base complexes

Nihal Deligönül and Mehmet Tümer*
Chemistry Department, Faculty of Science and Arts, K.Maras Sütcü Imam University, 46100 K.Maras, Turkey

Selahattin Serin
Chemistry Department, Faculty of Science and Arts, Cukurova University, 01100 Adana, Turkey

Received 5 May 2006; accepted 6 June 2006

Abstract

In this study, the Schiff base ligands H_2L^1–H_2L^3 and their Cu^{II}, Co^{II}, Ni^{II}, Fe^{III} Ru^{III} and VO^{IV} complexes have been prepared and characterized by spectroscopic and analytical techniques. All the complexes are mononuclear. Keto-enol tautomeric forms of the ligands have been investigated in polar and apolar solvents. The ligands favor the keto-form in the C_7H_8 and C_6H_{14}. The C–C coupling reaction of the 2,6-di-*t*-butylphenol has been investigated by the Co^{II} and Cu^{II} complexes. Thermal properties of the complexes have been assessed using thermal techniques and similar properties were found. In the Fe^{III} and Ru^{III} complexes, firstly, the coordinated water molecule is lost from the complex; in the second step, the chloride ion leaves the molecule in the 300–350 °C temperature range. Finally, the complexes decompose to the appropriate metal oxide at the higher temperature ranges. The electrochemical properties of the complexes have been studied in the two different solvents (DMF and CH_3CN).

Introduction

Transition metal complexes containing oxygen and nitrogen donor Schiff base ligands have been of research interest for many years [1–4], because of the versatility of their steric and electronic properties, which can be fine-tuned by choosing the appropriate amine precursors and ring substituents [5–9]. The value of these tetradentate N_2O_2 ligands and their transition-metal complexes, as catalysts, has attracted significant attention, being relevant for their applications, particularly on the development of agrochemical and pharmaceutical industries. Also, due to the potential catalytic interest of these metal-salen chelates, a very rapid growth in their chemical study has been developed, in view of a good characterization of their properties. A wide variety of cobalt(II) complexes are known to bind dioxygen more or less reversibly and are therefore frequently studied as model compounds for natural oxygen carriers and for their use in O_2 storage, as well as in organic syntheses due to their catalytic properties under mild conditions [10].

The recent use of salen complexes as catalytically active materials to develop surface-modified electrodes for sensoring applications has stimulated the use of the cyclic voltammetry as a technique to study the structure–reactivity relationships for this class of compounds [11]. Numerous electrochemical studies have been made for a fairly large number of acyclic and macrocyclic transition metal complexes derived from Schiff-bases. These investigations revealed that the redox properties of the complexes are markedly influenced by structural and electronic factors [12].

As salen has the desirable characteristic of being readily subject to systematic modification of its electronic and steric properties by synthetic approaches, we have prepared a series of the metal complexes with salen derivatives (H_2L^1–H_2L^3) that have different diimine bridges and same substituent in the aldehyde moieties (Scheme). Moreover, the C–C coupling, catalysis, electrochemical, thermal and spectroscopic properties of the transition metal complexes are herein reported.

Experimental

Materials

All metal salts and organic solvents were purchased from commercial sources and used as received, unless noted otherwise. 2,6-di-*t*-butylphenol, 2,4-di-hydroxy-

* Author for correspondence: E-mail: mtumer@ksu.edu.tr

benzaldehyde, ethylenediamine, 1,3-di-aminopropane and 1,4-di-aminobutane were purchased from Fluka.

Physical measurements

Elemental analyses (C, H, N) were performed using a LECO CHNS 932 (Inönü University, Malatya, Turkey) elemental analyser. I.r. spectra were obtained using KBr discs (4000–400 cm^{-1}) on a Shimadzu 8300 FT-IR spectrophotometer. The electronic spectra in the 200–900 nm range were obtained on a Shimadzu UV-160 A spectrophotometer. Magnetic measurements were carried out by the Gouy method using $Hg[Co(SCN)_4]$ as calibrant. Molar conductances of the Schiff base ligands and their transition metal complexes were determined in MeOH ($\sim 10^{-3}$ M) at room temperature using a Jenway Model 4070 conductivity meter. Mass spectra of the ligands were recorded on a VG ZabSpec GC-MS spectrophotometer (TUBITAK) with fast atom bombardment. ^{1}H- and ^{13}C-n.m.r. spectra were recorded on a Varian XL-200 instrument. TMS was used as internal standard and deuteriated DMSO-d_6 as solvent. The metal and chloride contents of the complexes were determined gravimetrically according to the known procedure [13]. The thermal analyses studies of the complexes were performed on a Perkin Elmer Pyris Diamond DTA/TG Thermal System under nitrogen atmosphere at a heating rate of 10 °C/min. Catalysis experiments were monitored on a Shimadzu 160-A UV–vis spectrophotometer with a data station. Experiments were carried out using methanol as solvent. In a generalized procedure a MeOH solution of 2,6-di-*t*-butylphenol (0.05 mM) and the metal complexes in a 50 cm^3 standard flask were kept under N_2. The compound 2,6-di-*t*-butylphenol (DTBP) was oxidized by aerial oxygen quantitatively to the 3,3′-5,5′-tetra-*t*-butyl-4,4′diphenoquinone (TTBD) by using the Cu^{II} and Co^{II} transition metal complexes as a catalyst. The change in the concentration of product 3,3′-5,5′-tetra-*t*-butyl-4,4′-diphenoquinone was monitored by optical spectroscopy.

Electrochemical studies were carried out with a Iviumstat Electrochemical workstation equipped with a low current module (BAS PA-1) at a platinum disk electrode and a platinum microelectrode of 10 μm diameter (BAS). Cyclic voltammetric measurements were made at room temperature in an undivided cell (BAS model C-3 cell stand) with a platinum counter electrode and an Ag/AgCl reference electrode (BAS). All potentials are reported with respect to Ag/AgCl. The solutions were deoxygenated by passing dry nitrogen through the solution for 30 min prior to the experiments, and during the experiments the flow was maintained over the solution. Digital simulations were performed using DigiSim 3.0 for windows (BAS, Inc.). Experimental cyclic voltammograms used for the fitting process had the background subtracted and were corrected electronically for ohmic drop.

Preparation of the ligands

All ligands were prepared by a similar method. Solutions of 2,4-dihydroxybenzaldehyde (2 mmol, in 20 cm^3 EtOH) and amine derivatives (1 mmol, in 20 cm^3 EtOH) were mixed together and refluxed for about 1 h on a water bath. The precipitated product was filtered and washed with cold EtOH (Figure 1). The ligands were recrystallized from $CHCl_3$/EtOH (1:3 by vol) and dried in the vacuum dessiccator over P_2O_5. The purity was checked by elemental analyses and melting point determination.

H_2L^1: ^{1}H-nmr: (DMSO-d_6 as solvent, δ in ppm): 15.65, 10.5(s, OH, 2H), 8.30 (s, CH=N, 2H), 6.66–7.30(m, Ar–H, 6H), 2.22 (t, CH_2, 4H). ^{13}C-nmr: (DMSO-d_6 as solvent, δ in ppm): 166.0 (CH=N), 110.2–150.6 (Ar–C), 58.5 (–CH_2–). Electronic spectra (λmax, nm): EtOH; 238, 282, 303, 377, 376. MeOH; 239, 280, 312, 374. C_7H_8; 266, 303, 315, 346, 394. C_6H_{14}; 253, 281, 313, 375, 388.

H_2L^2: ^{1}H-nmr: (DMSO-d_6 as solvent, δ in ppm): 13.33, 9.8 (s, OH, 2H), 8.40 (s, CH=N, 2H), 6.0–7.20(m, Ar–H, 6H), 1.80–3.50 (t, CH_2, 4H; p, CH_2, 2H). ^{13}C-nmr: (DMSO-d_6 as solvent, δ in ppm): 164.0 (CH=N), 108.5–136.6 (Ar–C), 56.1 (–CH_2–), 34.5 (–CH_2–). Electronic spectra(λmax, nm): EtOH; 242, 281, 306, 375. MeOH; 280, 306, 374. C_7H_8; 227, 261, 287, 315, 347, 399. C_6H_{14}; 240, 276, 391.

H_2L^3: ^{1}H-nmr: (DMSO-d_6 as solvent, δ in ppm): 14.70, 10.5 (s, OH, 2H), 8.80 (s, CH=N, 2H), 6.6–7.70(m, Ar–H, 6H), 1.20–2.10 (t, CH_2, 4H; p, CH_2, 4H). ^{13}C-nmr: (DMSO-d_6 as solvent, δ in ppm): 166.6 (CH=N), 109.2–148.1 (Ar–C), 55.5 (–CH_2–), 32.0 (–CH_2–). Electronic spectra(λmax, nm): EtOH;

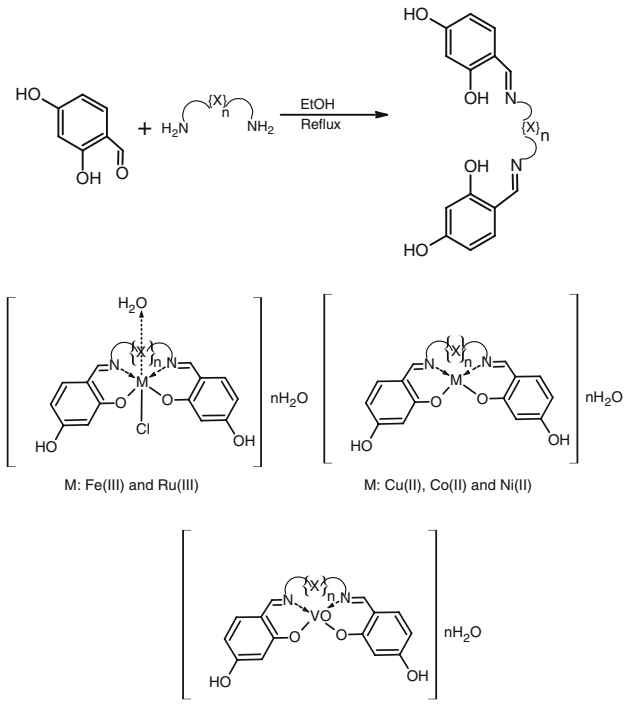


Fig. 1. Proposed structure of the ligands and their metal complexes.

243, 280, 305, 374. MeOH; 244, 288, 302, 372. C_7H_8; 208, 261, 290, 304, 315, 346, 357, 387. C_6H_{14}; 243, 282, 354, 397.

Preparation of the complexes

The complexes were prepared by similar methods. A solution of the metal salt (1 mmol) in absolute MeOH (25 cm^3) was added to a solution of the H_2L^1–H_2L^3 ligands (1 mmol) in absolute MeOH (20 cm^3) and the mixture was boiled under reflux for 6–7 h. At the end of the reaction, determined by t.l.c., the precipitate was filtered off, washed with distilled water and then EtOH, and dried *in vacuo*.

Catalytic oxidation of 2,6-di-t-butylphenol

In a CH_2Cl_2/MeOH solvent mixture (1:1, 50 cm^3), the complexes Cu^{II} and Co^{II} were dissolved. To it 2,6-di-*t*-butylphenol was added and the solution was stirred for 48 h. The solution was then filtered and the filtrate was evaporated to dryness. About 5 cm^3 of MeOH were added to dissolve the excess 2,6-di-*t*-butylphenol. For measuring the progress of the reaction, 50 μl from the aliquot was passed through an Amberlyst cationic ion-exchanger and washed with 10 cm^3 (2 × 5) CH_2Cl_2. The change in the concentration of product 3,3′-5,5′-tetra-*t*-butyl-4,4′-diphenoquinone was monitored by optical spectroscopy.

Results and discussion

We have prepared and characterized the six type complexes (N,N′-*bis*-(*o*-amidobenzilidene)-1,3-diaminopropane) and $[M(L^1)H_2O(X)]nH_2O$, (N,N′-*bis*-(*o*-amido benzilidene)-1,4-diaminobutane) $[M(L^2)H_2O(X)]nH_2O$ and (N,N′-*bis*-(*o*-thiobenzilidine)-1,4-diaminobutane) Cu^{II}, Co^{II}, Ni^{II}, VO^{IV}, Fe^{III} and Ru^{III} $[M(L^3)H_2O(X)]nH_2O$ [X: Cl^- for Fe^{III} and Ru^{III}], thus completing the series of metal complexes with 1,2-ethane, 1,3- propane and 1,4-butane backbones with N_2O_2 donor sets. We characterized tetradentate Schiff base metal(II)/(III) complexes by using UV–vis, IR, DTA/TGA, $^1H(^{13}C)$-NMR, mass spectra and elemental analysis. The elemental analysis (Table 1) of the Schiff base ligands and their M(II)/(III) complexes agree well with the composition of the proposed complexes and support the fact that the mole ratio of Schiff base ligands to the M(II)/(III) metal is 1:1 as shown in Figure 1. All the complexes are stable in air at room temperature, non-hygroscopic in nature and highly soluble in common solvents such as CH_2Cl_2, CH_3CN, $CHCl_3$ and DMSO producing intense color solutions. The more the solubility of the complexes is may be due to the free hydroxyl groups on the benzene ring. The conductivity data in 1 mM methanol solution indicate that the M(II)/(III) complexes are non-ionic compounds. For transition metals capable of adopting higher coordination numbers, such as Ru^{III} and Fe^{III} the ability of the larger ring sizes generated by N,N′-*bis*-(4-hydroxysalicylidene)-1,2-diaminoethane (H_2L^1), N,N′-*bis*-(4-hydroxysalicylidene)-1,3-diaminopropane (H_2L^2) and N,N′-*bis*-(4-hydroxysalicylidene)-1,4-diaminobutane (H_2L^3) complexes would seem to support the formation of a wider range of geometries. The advantages of working with VO(Salen) are the high stability of the complex and simple synthesis from commercially available $VOSO_4{\cdot}5H_2O$. The hydroxy group in the *ortho* and *para* position on each salicylidene unit was added to reinforce the stability of the metal complex and to create a hydroquinone system cooperating with the metal redox system.

The free Schiff base ligands show a very strong absorption in the 1647–1641 cm^{-1} range in their IR spectra which are characteristic of the azomethine ν(C=N) group (Table 2). In the Schiff base complexes, this absorption has been shifted to the 1624–1612 cm^{-1} region indicating the coordination of the Schiff bases through the nitrogen atom. In all the complexes the bands appeared in the 1547–1553 cm^{-1} region and have been assigned to the mixed mode of vibration arising from ν(C=N) and ν(C=C) vibrations [14]. This also indicates that the coordination is through the nitrogen atom. Moreover, the absorptions due to ν(C–O) of the ligands in the 1365–1283 cm^{-1} range are shifted to the 1363–1319 cm^{-1} range in the complexes, indicating that the other coordination is through the phenolic oxygen atom. In the complexes containing water molecules in the empirical formula, the absorptions due to O–H stretching and ν(O–H) bending vibrations are observed at 3500 cm^{-1} and 1300 cm^{-1}, respectively, indicating the presence of water molecules. A strong band in the 1304–1344 cm^{-1} region is associated with the stretching frequency of the ν(V–O) (phenolic) bond. A strong ν(V=O) stretching band, appearing in the 967–970 cm^{-1} region in all the complexes, indicates the tetracoordinated environment around the metal center.

The electronic spectra of the complexes were recorded in MeOH and the obtained data are given in Table 2. The bands in the 200–390 nm region coincide with the bands observed in the free ligands. Two relatively less intense bands occur in the 390–450 nm region. These can be assigned to phenolic oxygen, to metal and imine nitrogen and to the metal charge transfer transitions, respectively. The electronic spectra of these Schiff base Cu^{II} complexes show very intense absorption bands in the UV region, attributed to ligand transitions ($n \rightarrow \pi^*$ and $\pi \rightarrow \pi^*$), and a characteristic broad band in the 687–564 nm range due to d–d transitions. Additionally, they showed a band in the 327–394 nm range, attributed to a LMCT transition, π(imine) $\rightarrow Cu^{II}$. The electronic spectra of the complexes are strongly dominated by the electronic transitions due to the iron–salicylaldiminate chromophores. The charge transfer bands from phenolate to the metal (causing the red–purple color of the complexes) are of

intermediate intensity and appear near 450 nm. These bands correspond to a charge transfer from the pπ orbital of phenolic oxygen to the dπ orbital of the iron. The absorption bands between 230 and 260 nm are assigned to π–π* transitions of benzenoid type [15].

The ground state of Ru^{III} is $^2T_{2g}$ and the first excited doublet levels in the order of increasing energy are $^2A_{2g}$ and $^2T_{1g}$ which arises from the $t^4{}_{2g}e_g{}^1$ configuration. In most of the ruthenium(III) complexes the electronic spectra show only charge transfer bands. Since in a d^5 system and especially in Ru^{III} which has relatively high oxidizing properties, the charge transfer bands of the type $L_{\pi y} \rightarrow t_{2g}$ are prominent in the low energy region which obscure the weaker bands due to d–d transition. It is therefore, difficult to assign conclusively the bands of Ru^{III} complexes which appear in the visible region. The electronic spectra of all the complexes in methanol showed two to four bands in the 478–223 nm region. The bands in the 478–223 nm region have been assigned to charge transfer transitions. Similar observations also have been made for other Ru^{III} complexes.

The brown–red tetravalent oxo-vanadyl(IV) complexes display two ligand-field transitions (Table 2) in the visible region: one near 600 nm and another near 410 nm, due to $d_{xy} \rightarrow d_{xz}$, d_{yz} and $d_{xy} \rightarrow d_{x^2-y^2}$ transitions. Strong absorptions at lower energies vitiate the other possible transition, $d_{xy} \rightarrow d_{z^2}$. There are also other two bands in the higher energy region for these four complexes: one at ~370 nm and another at ~310 nm due to O(phenolic) $\rightarrow V^{4+}$ and $\pi \rightarrow \pi'$ (of the C=N bond) transitions [16], respectively. For six coordinate Fe^{III} complexes, all d–d transitions are forbidden and hence, generally, for the synthesized Fe^{III} complex, absorption bands are not observed.

The molar conductivity data of all compounds in MeOH (~10^{-3} M solutions) are given in Table 1. The conductivity data of the ligands and their complexes are very low and they can be regarded as non-electrolytes.

We have also examined the catalytic activities of the complexes $[M(L^n)]nH_2O$ (M = Cu^{II} and Co^{II}) for oxidation of 2,6-di-*t*-butylphenol by air O_2 to 2,2′-di-*t*-butyl-4,4′-diphenolquinone (DTBD) in air saturated DCM according to the reaction in the Scheme. All complexes in the catalysis reaction are soluble in the DCM–methanol solvent mixture. If they are not also soluble in this mixture, there is not any problem. Because, this type reaction can occur at the heterogenous or homogenous phase in the similar way. When the sterically hindered phenol (2 mmol) are added to the complexes (0.01 mmol) in DCM–methanol (1:1) solvent mixture (50 ml), the dark brown or black colors turn to red or light red in presence of air. It was found that after 50–80 h, 100% phenols were converted to the 3,3′-5,5′-tetra-*t*-butyl-4,4′-diphenolquinone for the complexes. The mechanism is reported in Scheme and involves the formation of a μ-peroxo-quinolato-cobalt(III) complex (2) from an initially formed phenoxyl radical and the metal–oxygen adduct (1) [17]. The cobalt peroxidic intermediate is the precursor of the quinone (1) and the competitive reaction of coupling of the phenoxy radicals will form the dimer DBQ (1). On these bases, the complex $[Co(L^3)]H_2'$ should be expected to convert less substrate than $[Co(L^2)]H_2O$ and $[Co(L^1)]2H_2O$. In addition, the $[Co(L^3)]H_2O$ has the highest chelate cavity (butyl chain) between $[Co(L^2)]$-H_2O and $[Co(L^1)]2H_2O$ as far as the electron density brought by the ligand system on the metal centre is concerned. Moreover, the presence of the consecutive

Table 1. Analytical and physical data of the Schiff base ligands and their metal complexes

Compound	Color	Yield (%)	M.p. (°C)	Found (calcd.)%				
				C	H	N	M	[a]M_M
H_2L^1	yellow	87	180	64.0 (64.0)	5.3 (5.4)	9.3 (9.3)	–	1.5
$[Cu(L^1)]2H_2O$	brown	70	> 250	48.2 (48.3)	4.4 (4.5)	7.1 (7.0)	16.0 (15.9)	7.8
$[Co(L^1)]2H_2O$	black	64	> 250	48.7 (48.8)	4.5 (4.6)	7.2 (7.1)	15.0 (14.9)	7.5
$[Ni(L^1)]H_2O$	dark brown	68	> 250	51.1 (51.2)	4.3 (4.2)	7.5 (7.4)	15.7 (15.6)	8.0
$[VO(L^1)]H_2O$	dark red	67	> 250	50.0 (50.1)	4.1 (4.2)	7.4 (7.3)	13.4 (13.3)	7.7
$[Ru(L^1)Cl(H_2O)]2H_2O$	black	71	> 250	40.7 (40.8)	4.3 (4.2)	5.8 (5.9)	21.6 (21.5)	6.9
$[Fe(L^1)Cl(H_2O)]2H_2O$	green	70	225	43.2 (43.3)	4.6 (4.5)	6.4 (6.3)	12.7 (12.6)	7.5
H_2L^2	orange	90	152	64.9 (65.0)	5.8 (5.7)	8.9 (8.8)	–	1.4
$[Cu(L^2)]2H_2O$	brown	68	225	49.7 (49.6)	4.8 (4.9)	6.7 (6.8)	15.5 (15.4)	8.0
$[Co(L^2)]H_2O$	dark brown	65	> 250	52.5 (52.4)	4.5 (4.6)	7.1 (7.2)	15.2 (15.1)	7.6
$[Ni(L^2)]H_2O$	brown	66	> 250	52.5 (52.4)	4.5 (4.6)	7.1 (7.2)	15.2 (15.1)	8.1
$[VO(L^2)]H_2O$	brown	72	> 250	51.2 (51.3)	4.6 (4.5)	7.1 (7.0)	12.9 (12.8)	6.5
$[Ru(L^2)Cl(H_2O)]$	black	68	200	43.8 (43.7)	3.9 (3.9)	5.9 (6.0)	21.7 (21.6)	7.4
$[Fe(L^2)Cl(H_2O)]3H_2O$	black	67	189	42.8 (42.9)	5.1 (5.0)	5.8 (5.9)	11.8 (11.7)	7.2
H_2L^3	yellow	90	232	65.8 (65.9)	6.1 (6.2)	8.5 (8.4)	–	1.7
$[Cu(L^3)]H_2O$	brown	69	> 250	52.6 (52.7)	5.3 (5.4)	6.9 (6.8)	15.6 (15.5)	8.2
$[Co(L^3)]H_2O$	brown	70	> 250	53.4 (53.3)	5.3 (5.4)	6.8 (6.9)	14.6 (14.5)	9.0
$[Ni(L^3)]2H_2O$	green	65	> 250	51.0 (51.1)	5.1 (5.2)	6.7 (6.6)	14.0 (13.9)	8.5
$[VO(L^3)]2H_2O$	black	70	> 250	50.0 (50.1)	5.0 (5.1)	6.6 (6.5)	11.9 (11.8)	10.0
$[Ru(L^3)Cl(H_2O)]2H_2O$	brown	67	> 250	41.7 (41.8)	4.7 (4.6)	5.3 (5.4)	19.6 (19.5)	9.5
$[Fe(L^3)Cl(H_2O)]2H_2O$	black	68	> 250	45.7 (45.8)	5.0 (5.1)	5.0 (5.9)	11.9 (11.8)	10.8

[a]Ω^{-1} cm^2 mol^{-1}.

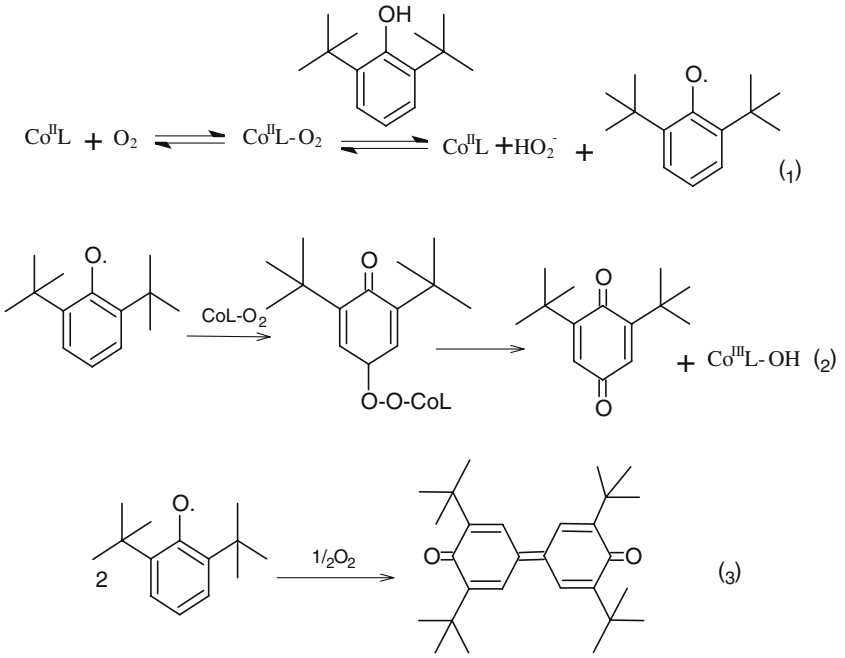
Table 2. Magnetic, infrared[a] and electronic spectral data of the Schiff base ligands and their metal complexes

Compound	ν(OH)	ν(N···H–O)	ν(CH=N)	ν(C–OH)	ν(M–N)	ν(M–O)	λ_{max}(nm, MeOH)	μeff (B.M.)
H_2L^1	3448	2505	1641	1356	–	–	239, 280, 312, 374	–
$[Cu(L^1)]2H_2O$	3421	2663	1614	1336	462	547	284, 300, 340, 366, 564	1.80
$[Co(L^1)]2H_2O$	3452	2577	1620	1336	461	567	264, 302, 363, 387, 610	4.23
$[Ni(L^1)]H_2O$	3422	2621	1620	1331	424	495	294, 387, 394, 431, 623	Diamag.
$[VO(L^1)]H_2O$	3414	2630	1614	1331	420	590	286, 305, 403, 584	1.74
$[Ru(L^1)Cl(H_2O)]2H_2O$	3452	2576	1624	1331	424	597	294, 325, 368, 578	1.79
$[Fe(L^1)Cl(H_2O)]2H_2O$	3413	2617	1618	1332	424	564	291, 299, 388, 466, 470	5.62
H_2L^2	3419	2609	1643	1365	–	–	280, 306, 374	–
$[Cu(L^2)]2H_2O$	3414	2360	1616	1338	462	547	295, 299, 327, 687	1.81
$[Co(L^2)]H_2O$	3414	2360	1618	1329		–	294, 299, 350, 356, 366, 625	4.20
$[Ni(L^2)]H_2O$	3414	2621	1618	1334	420	547	294, 297, 302, 373, 612	Diamag.
$[VO(L^2)]H_2O$	3414	2336	1616	1334	462	634	294, 295, 305, 409, 609	1.75
$[Ru(L^2)Cl(H_2O)]$	3420	2360	1618	1319	–	648	285, 302, 378, 571	1.80
$[Fe(L^2)Cl(H_2O)]3H_2O$	3415	2360	1618	1323	420	528	294, 302, 382, 401	5.54
H_3L^3	3423	2497	1647	1283	–	–	244, 288, 302, 372	–
$[Cu(L^3)]H_2O$	3419	2360	1612	1321	420	500	299, 357, 364, 394, 615	1.79
$[Co(L^3)]H_2O$	3419	2586	1618	1363	466	528	302, 350, 370, 392, 614	4.24
$[Ni(L^3)]2H_2O$	3413	2624	1616	1331	420	526	294, 297, 302, 405, 621	Diamag.
$[VO(L^3)]2H_2O$	3421	2354	1616	1342	420	570	295, 373, 425, 586	1.74
$[Ru(L^3)Cl(H_2O)]2H_2O$	3420	2361-	1618	1329	424	547		1.76
$[Fe(L^3)Cl(H_2O)]2H_2O$	3415	2360	1618	1323	420	501		5.61

[a] cm^{-1}.

equilibrium [Eq. (2)] should lower the concentration of the active species. These effects both play in the direction of a decreased catalytic activity. On the contrary, it is found that the three systems show similar initial and final conversions and are deactivated approximately after the same time. Therefore, the dimerization [Eq. (2)] of the $[Co(L^3)]H_2O$ system does not decrease, as expected, the catalytic performance of the catalyst. Under the experimental conditions here adopted, the dimerization has not the time to proceed and, likely, $[Co(L^3)]H_2O$ behaves simply as a complex which forms with dioxygen only the mononuclear adduct described in reaction (Scheme 1).

For the compound 2,6-di-*t*-butylphenol, the best oxidants: are the complexes of the ligand H_2L^1. Moreover, the complexes of the ligands H_2L^3 and H_2L^2 are the worst oxidant for the sterically hindered phenol. These two different situations can be explained by the properties of the ligands. The chalete ring sizes of this ligands are greater than the ligand H_2L^1. In all ligands, in the p-position of the carbonyl fragments of the ligands, there are the –OH groups, and because of this group has the electron-donor property with mesomeric effect, the activity of the complexes increases. The complexes Co^{II} of the ligands show better catalytic activity than the Cu^{II} complexes. Larger atomic



Scheme 1.

radius of the Cu^{II} ion may be due to this situation, because, interaction of the complex and phenol may be hard because of steric hindrance. Order of the oxidizing of the complexes is:

$$[Co(L^1)]2H_2O > [Co(L^2)]H_2O > [Co(L^3)]H_2O > [Cu(L^1)]2H_2O > [Cu(L^2)]2H_2O > [Cu(L^3)]H_2O.$$

The conservation ratio (as %) of 2,6-di-*t*-butylphenol to the TTBD is shown in Figure 2. In the reactions catalyzed by the Co^{II} and Cu^{II} complexes, the conservation product TTBD is obtained for the Co^{II} complexes in the highest yield. The course of the reaction was also followed by optical spectroscopy, as TTBD shows a characteristic peak in the electronic spectrum at 425 nm. Such changes in the electronic spectra of the complexes at different time intervals were monitored by removing the catalyst from the reaction solution. At the end of the oxidative coupling , the properties of the complexes change.

^{1}H- and ^{13}C-NMR spectra

The ^{1}H- and ^{13}C-n.m.r. spectra of the ligands have been recorded in DMSO-d_6 as solvent. Obtained data are given in the experimental section. The tetradentate Schiff base ligands possess two phenolic and azomethine groups. In the spectra of the ligands, the $-CH_2-$ groups in the 1.0–3.8 ppm range is shown as only a triplet (for H_2L^1), triplet and pentet (for H_2L^2 and H_2L^3). ^{1}H-nmr spectra in DMSO-d_6 showed the aromatic protons as multiplet in the range 6.00–7.70 ppm and OH protons of the two phenolic groups in the range 9.60–10.20 ppm and 13.33–15.65 ppm. The azomethine protons appeared as a sharp singlet in the range 8.30–8.90 ppm. The complexes did not show two phenolic protons, but show only one signal in the range 13.35–15.70 ppm. Moreover, the azomethine protons of the free ligands are shifted downfield to 9.15–9.80 ppm on complexation. These observations suggest that the ligands coordinate to the metal ion through the phenolic oxygen and nitrogen atoms of the azomethine group (Figures 3 and 4).

In the ^{13}C-n.m.r. spectra of the ligands, the peaks in the 136.4–145.5 ppm range are due to the C-2 and 4 nuclei for the ligands which are attached to the hydroxyl groups. The ^{13}C-n.m.r. spectra of the all ligands showed 8, 9 and 10 peaks for H_2L^1, H_2L^2 and H_2L^3, respectively, as expected. The greatest downfield peak in δ 161.2–164.5 ppm range for the fress ligands are likely to arise from the C-7 resonance (Figure 5).

The keto-enol tautomeric forms of the Schiff base ligands are seen in Figure 6. In order to study the tautomeric properties of the ligands, the electronic spectra were recorded in the EtOH, MeOH, C_6H_{14} and C_7H_8 solvents. The obtained data are given in the experimental section. The structures of this kind of Schiff base, which are widely used as chelating agents, are relevant due to the possibility of finding them in the solid state and/or in solution as keto-amine or phenolimine tautomers, and their connections with photochromism and thermochromism. In the solid state, salicylaldimine Schiff bases tend to form (N···H–O) or (N–H···O) types of hydrogen bonding, respectively. In many cases in solution, both types of hydrogen bonds have been observed indicating phenol-imine, O–H···N, keto-amine, O···H–N tautomerism [18, 19]. Knowing the structures of free Schiff bases in solution and in the solid state is important in view of the intramolecular hydrogen bonding and comparison with the struc-

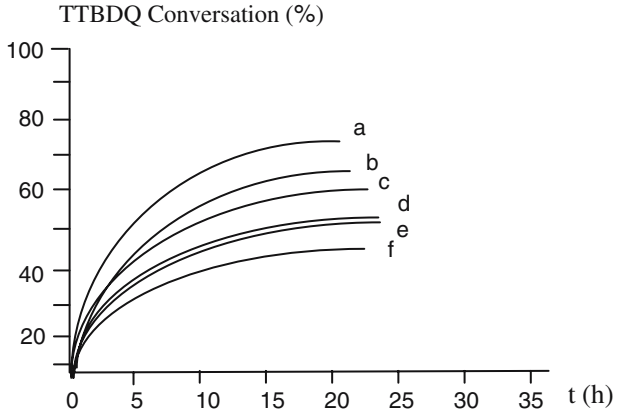


Fig. 2. The electronic spectra of the complexes Cu^{II} and Co^{II} for the C–C coupling reaction of the 2,6-di-*t*-butylphenol. [a: $[Co(L^1)]2H_2O$, b: $[Co(L^2)]H_2O$, c: $[Co(L^3)]H_2O$, d: $[Cu(L^1)]2H_2O$, e: $[Cu(L^2)]2H_2O$, f: $[Cu(L^3)]H_2O$].

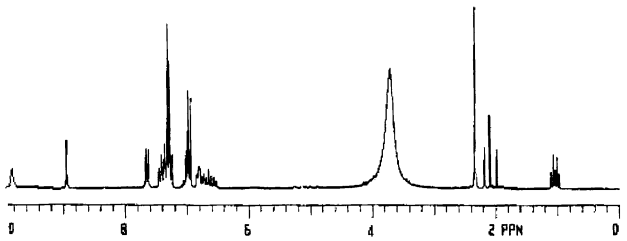


Fig. 3. ^{1}H-n.m.r. spectrum of the ligand H_2L^3.

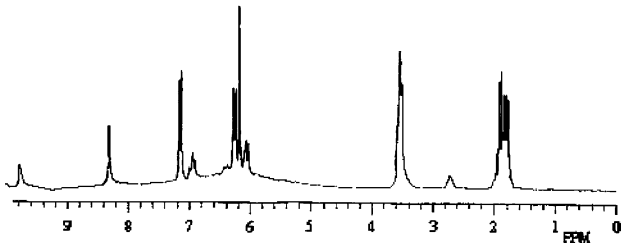


Fig. 4 ^{1}H-n.m.r. spectrum of the ligand H_2L^2.

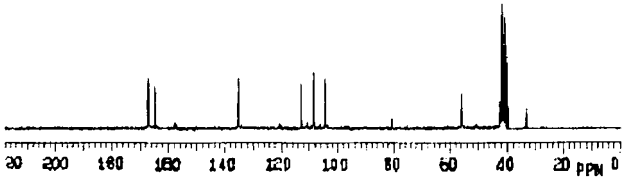


Fig. 5. ^{13}C-n.m.r. spectrum of the ligand H_2L^2.

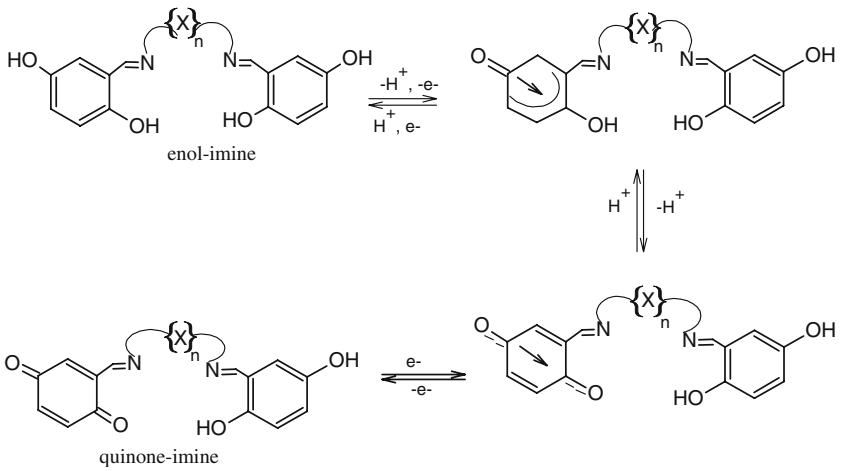


Fig. 6. Proposed tautomeric forms of the ligands.

ture of Schiff base complexes. In our synthesized ligands, in the apolar solvents (C_6H_{14} and C_7H_8), the ligands prefer the quinone-imine tautomeric form, because the value λ_{max} of the ligands shifted to the 387–399 nm range. In polar solvents (EtOH, MeOH), as ligands and solvent molecules form the intermolecular hydrogen bonding, the ligands prefer the enol-imine form (λ_{max} is in the range 372–376 nm in the EtOH and MeOH solution).

The magnetic moments (Table 2) of the paramagnetic complexes have been measured at room temperatures (298 K). The Ni^{II} complexes have diamagnetic character and show the square–planar geometry around the metal centres. The Cu^{II} complexes have a magnetic moment data in the 1.79–1.81 μ_B range and reveal that they have a distorted tetrahedral geometry around the metal ion. The magnetic moments of the Co^{II} complexes are in the 4.20–4.24 μ_B range and these data confirm that the Co^{II} complexes have a tetrahedral nature. The room temperature magnetic moments for the Fe^{III} and Ru^{III} complexes have been measured. The values obtained for the Fe^{III} complexes were in the 5.54–5.62 μ_B range, and these data are suitable for octahedral geometry. The magnetic moment data for the Ru^{III} complexes are in the 1.76–1.80 μ_B range. The magnetic moment values of the Ru^{III} correspond to one unpaired electron suggesting a low spin t^5_{2g} configuration for the Ru^{III} ion in an octahedral environment. The oxo-vanadyl(IV) complexes $[VO(L^1)]H_2O$, $[VO(L^2)]H_2O$ and $[VO(L^3)]2H_2O$ have the magnetic susceptibility data 1.74, 1.75 and 1.74 μ_B, respectively, and these data confirm that the complexes have the square–pyramidal nature around the metal ion.

In the mass spectra of the ligands H_2L^1, H_2L^2 and H_2L^3, the signals in the 300, 314 and 328 can be attributed to the molecular ion $[M]^+$ peaks, respectively.

The thermal behavior of the complexes were characterized using DTA and TGA/DTG methods. The DTA/TG measurements of the complexes were carried out in the 20–1000 °C range. Typical thermograms of the complexes $[Fe(L^1)Cl(H_2O]2H_2O$ and $[Fe(L^2)Cl(H_2O]3H_2O$ are shown in Figures 7 and 8, respectively. The complexes were stable up to the loss of the adsorbed water molecules. In the complexes, the outer water molecules are removed in the 40–80 °C temperature range with an endothermic process that lead to non-isolable complexes. Up to 100 °C, the complexes containing the adsorbed water molecules loss approximately 4.60–9.11% of their mass. The complexes $[M(L^n)Cl(H_2O)]nH_2O$ (M: Fe and Ru) contain the coordinated chloride ion and water molecules.

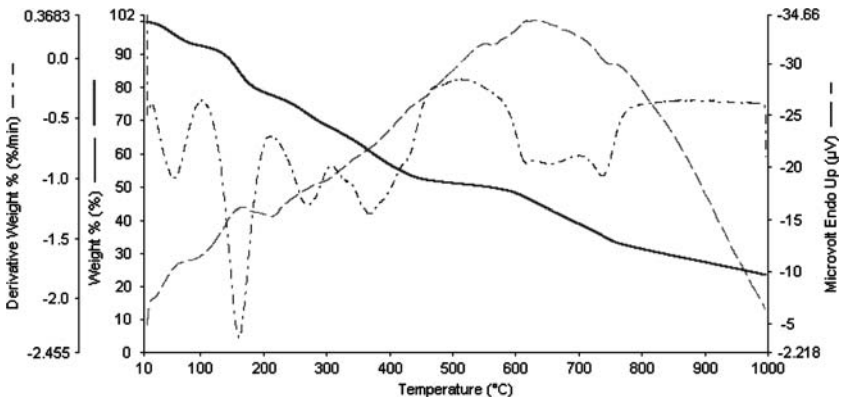


Fig. 7. Thermogram of the complex $[Fe(L^1)Cl(H_2O]2H_2O$.

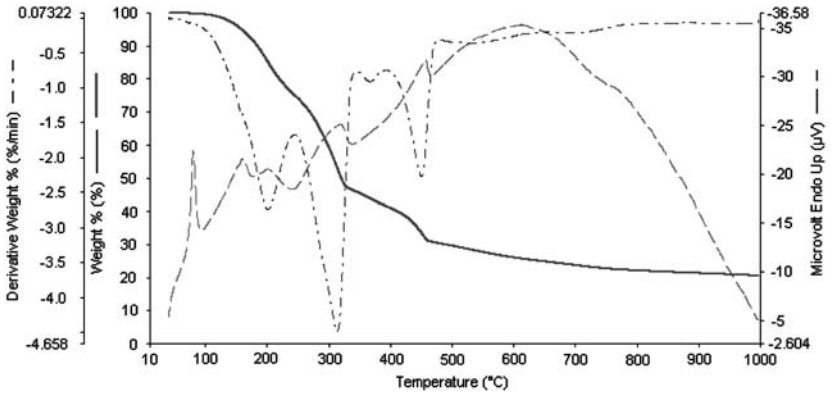


Fig. 8. Thermogram of the complex $[Fe(L^2)Cl(H_2O]3H_2O$.

There is one route in removal of coordinated water molecules in the 150–200 °C temperature range from the complexes. This mass loss equals the 3.75–4.55% of the total mass. Moreover, the coordinated chloride ion loss from the complexes in the 280–300 °C temperature range. At the higher temperatures (450–800 °C), all complexes decompose to give the appropriate metal oxide. The lower stability of the Co^{II} complex might be attributed to the autocatalytic effect of the Co^{II} ion. In addition, intermolecular factors may operate and control the stability of the complexes. In addition, the coordinated and non-coordinated water molecules have a weak ligand character.

The factors affecting the thermal stability of transition metal complexes in the solid state are not well understood. There are many examples in which the following order of thermal stability was established: Mn > Fe > Co > Ni > Cu < Zn. This is the reverse of the Irwing–Williams series, *i.e.* the stability order of the complexes in aqueous solution. This behavior can be explained by a decrease of the intermolecular forces in the solid state with increasing strenght of the intramolecular metal–ligand bonds. In the complexes, the following thermal stability order can be recognized:

Fe > Ni > Cu > Ru > Co > VO.

Electrochemistry

The redox properties of all the Ru^{III} complexes were investigated in DMF solution (in a nitrogen atmosphere) by cyclic voltammetry and the redox processes are metal centered only (Table 3). Cyclic voltammograms of all the complexes (1×10^{-3} M) exhibit a reversible oxidation and reversible reduction peaks at the scan rate 100 mV s^{-1}. A representative cyclic votammogram of $[Ru(L^3)Cl(H_2O)]2H_2O$ is shown in Figure 9. All the complexes showed well-defined waves in the range ($E_{1/2}$) + 0.215 to +0.445 V (Ru^{IV}/Ru^{III}) and 0.015–0.027 V (Ru^{III}/Ru^{II}) *versus* Ag/AgCl. The redox processes are reversible with peak-to-peak separation (ΔE_p) values ranging from 60 to 80 mV corresponding to one-electron process. For scan rate 100 mV s^{-1}, the ratio *i*p/SR (*i*p = peak current;

Table 3. Electrochemical data of the Schiff base complexes

Complexes	E_{pa} (V)	E_{pc} (V)	$E_{1/2}$ (mV)	E_p (mV)
$[Cu(L^1)]2H_2O$	0.530	0.620	0.575	−90
$[Co(L^1)]2H_2O$	−0.690	−0.390	−0.540	−300
$[Ni(L^1)]H_2O$	−0.500	−0.210	−0.355	−290
$[VO(L^1)]H_2O$	0.015, 0.350	0.465, 0.880	0.405	−115
$[Ru(L^1)Cl(H_2O)]2H_2O$	0.110, 0.850	0.095	0.015, 0.445	755
$[Fe(L^1)Cl(H_2O)]2H_2O$	−0.470	−0.710	−0.590	240
$[Cu(L^2)]2H_2O$	0.380	0.610	0.495	−230
$[Co(L^2)]H_2O$	−0.570	−0.400	−0.485	−170
$[Ni(L^2)]H_2O$	−0.650	−0.460	−0.555	−190
$[VO(L^2)]H_2O$	0.010, 0.420	0.470, 0.930	0.430	50
$[Ru(L^2)Cl(H_2O)]$	0.112, 0.904	0.085	0.027, 0.215	819
$[Fe(L^2)Cl(H_2O)]3H_2O$	−0.505	−0.730	−0.640	225
$[Cu(L^3)]H_2O$	0.37	0.580	0.475	−210
$[Co(L^3)]H_2O$	−0.640	−0.410	−0.525	−230
$[Ni(L^3)]2H_2O$	−0.80	−0.45	−0.625	−350
$[VO(L^3)]2H_2O$	0.380, 0.08	0.445, 0.960	0.412	−65
$[Ru(L^3)Cl(H_2O)]2H_2O$	0.114, 0.785	0.088	0.016, 0.436	797
$[Fe(L^3)Cl(H_2O)]2H_2O$	−0.510	−0.740	−0.625	230

Supporting electrolyte: $[NBu_4](ClO_4)$ (0.05 M); concentration of the complex: 0.001 M; scan rate: 100 mV s^{-1}. All the potentials are referenced to Ag/AgCl; where E_{pa} and E_{pc} are anodic and cathodic potentials, respectively. $E_{1/2} = 0.5 \times (E_{pa} + E_{pc})$, $\Delta E_p = E_{pa} - E_{pc}$.

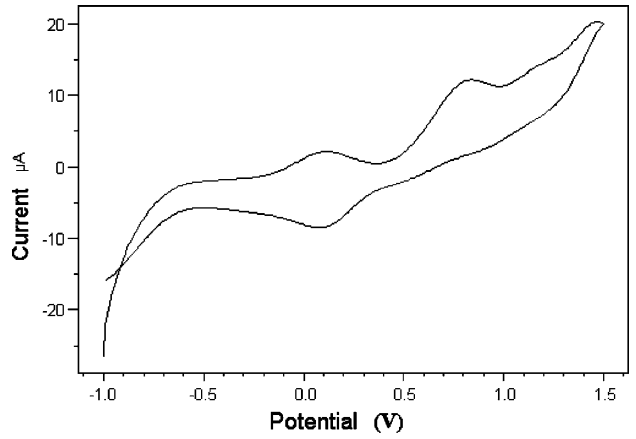


Fig. 9. Cyclic voltammetry of $[Ru(L^3)Cl(H_2O)]$ in DMF in the presence of tetrabutylammonium hexafluorophosphate (0.1 M).

sr = scan rate) was approximately one, the peak separation being independent of the scan rate. This indicates that the electron transfer is reversible and the mass transfer is limited. It has been observed that some of the complexes show quasireversible redox processes which did not change with change in scan rates, supporting reversibility. The electron donating group (–OH) as the mesomeric effect ability of the substituent on the phenyl ring of the Schiff base favored oxidation of Ru^{III} to Ru^{IV} [20].

$$[Ru^{III}(L^3)Cl(H_2O)] \leftrightarrow [Ru^{IV}Cl(H_2O)(L^3)]^+ + e^-$$

The redox properties of the Cu^{II} complexes were investigated in DMF by cyclic voltammetry and the redox processes are metal centered only (Table 3). Cyclic voltammogram of all the complexes (1×10^{-3} M) exhibit a reversible oxidation and reversible reduction peaks at the scan rate 100 mV s^{-1}. The behaviour of $[Cu(L^3)]H_2O$ is depicted in Figure 10 and is similar to that found for all copper complexes. One of the studied complexes, $[Cu(L^3)]H_2O$, showed reversible behavior, with ΔE_p (Cu^{II}–Cu^{I}) = −0.21 V (see Figure 10) in DMF solution containing tetrabutylammonium perchlorate (0.10 mol dm^{-3}). Similar results

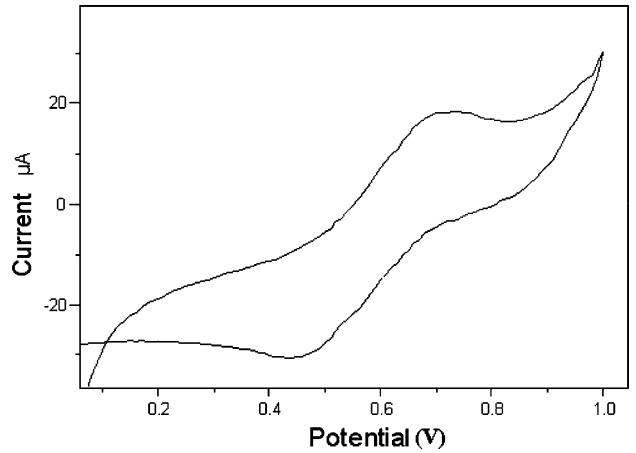


Fig. 10 Cyclic voltammetry of the $[Cu(L^3)]H_2O$ in DMF in the presence of tetrabutylammonium hexafluorophosphate (0.1 M).

have been reported for $[Cu(L^1)]2H_2O$ and other copper(II) complexes. For $[Cu(L^1)]2H_2O$, the reduction of Cu^{II} to Cu^{I} at more positive potential (−0.09 V) when compared to that of $[Cu(L^2)]2H_2O$, and $[Cu(L^3)]H_2O$, −0.23 and −0.21 V, respectively, is consistent with a co-ordination geometry intermediate between square planar and tetrahedral around the Cu^{II} ion. Besides, an unsaturated nitrogen as the donor atom in the ligand stabilizes more a low oxidation state, such as Cu^{I}, than a saturated one, by π-back bonding between the metal and the nitrogen atoms. If the cathodic scan is limited to the first reduction peak a quasi-reversible redox couple ($E_{1/2}$ = 0.575 V) is only observed.

This first reduction process is diffusion controlled with the cathodic current function ($I_{pc}/v^{1/2}$) independent of the scan rate (v) over the range 25–500 mV s^{-1}. The peak potentials separation is ΔE_p = −90 mV and the ratio of cathodic to anodic peak current is close to unity. The electrode processes can be described by the Eq. (1).

$$[Cu^{II}(L^3)]H_2O + e^- \rightarrow [Cu^{I}(L^3)]H_2O$$

The redox properties of the Co^{II} complexes were investigated in CH_3CN solution by cyclic voltammetry and the redox processes are metal centered only (Table 3). Cyclic voltammogram of all the complexes (1×10^{-3} M) exhibit a reversible oxidation and reversible reduction peaks at the scan rate 100 mV s^{-1}. One quasi-reversible redox couple is a common feature of the cyclic voltammograms of the complexes. The values of ΔE_p and peak current ratios of the waves are consistent with one-electron transfer processes. The $E_{1/2}$ values remain unchanged with different scan rates (25–500 mV s^{-1}), suggesting that the redox processes are uncoupled with any chemical reaction. The reduction wave at −0.8 V is assigned to the $Co^{II/I}$ couple.

A similar feature was also observed for $[Ni(L^3)]2H_2O$ at −0.80 V, and is assigned to the $Ni^{II/I}$ couple. Reduction of the nickel(II) complexes was found to be solvent independent, but on the other hand the final reduction product depends largely on the ligand diimine bridge. Complexes with aromatic diimine bridges yielded ligand-centred reduced species. Furthermore, the observation that the $E_{1/2}$ values for all complexes are practically solvent independent implies that the solvent does not participate in the charge transfer process, and indicates that the reduced nickel species must keep their tetra coordinate geometry. This result must be contrasted with the oxidation process of the same complexes, for which the solvent has a marked influence on oxidation site (metal and ligand), with good donor solvents favouring formation of the Ni^{III} complexes [21]. Electron-donating substituents as inductive or mesomeric (methylene group(s) on the chain and the OH group on the phenylene ring) are expected to decrease the values of $E_{1/2}$, and as such their $E_{1/2}$ values would be expected to be less positive than those of $[Ni(L^1)]H_2O$. However, the values obtained were more negative, an indication that steric constraints play a

more important role than electronic effects in the solution stability of the electrogenerated Ni^{III} species.

The cyclic voltammetry of the complex $[Fe(L^3)Cl(H_2O)]2H_2O$ in CH_3CN presents only one anodic reversible wave at $E_{1/2} = -0.623$ V. The same reversible wave is observed as a cathodic process in the cyclovoltammogram of the complex $[Fe(L^2)Cl(H_2O)]3H_2O$, demonstrating that it is associated to the monoelectronic transformation $Fe^{II} + e^- \rightarrow Fe^{III}$. Similar quasi-reversible processes have been observed for $[Fe(L^1)Cl(H_2O)]2H_2O$ at -0.590 V. The increase of the oxidation potential when going from the H_2L^1 complex to the H_2L^3 one may be attributed to the greater cavity of the amine substituent.

Electrochemical studies of the $[VO(L^x)]nH_2O$ were carried out in either CH_3CN or DMF solution by cyclic voltammetry at room temperature. Figure 11 shows the cyclic voltammograms of $[VO(L^3)]2H_2O$ in DMF solution at various scan rates. As can be seen in Figure 11, the redox processes were reversible, also the cathodic peak current of the complexes was increased and the peak potentials shifted to more negative direction with the increase of the scan rate. Compounds examined in both solutions (DMF, CH_3CN) showed small shifts of those redox potentials between solvents (< 0.01 V). The vanadyl complexes, $[VOL^x]nH_2O$; $x = 1$, 2 and 3 exhibit electrochemical properties. Overall, the V^V/V^{IV} reduction potential shifts by approximately 100 mV from the parent $[VOL^1]$ to $[VOL^3]$ (Table 3). The number of electrons transferred in the electrode reaction for a reversible couple can be determined from the separation between the peak potential.

$$\Delta E_p = E_{pa} - Epc = \frac{0.0591}{n}$$

where E_{pa}, E_{pc}, and n are anodic potential, cathodic potential and the number of electrons transferred, respectively. Thus, a one electron process exhibits a ΔE_p approximately 0.059 V. At slower scan rate, the peak separation for the cathodic and anodic cyclic votammetric peak potentials is very close to 60–70 mV, indicating that the number of electrons transferred should be 1.0. These results show that the electrochemical redox processes of vanadyl complexes with unsymmetrical Schiff base ligands are quasi-reversible charge transfer. Also, the oxidation potential for the complexes with the substituted ligands or longer chelate ring ($n = 3$) show less positive value than that of the complexes with unsubstituted ligands or shorter chelate ring ($n = 2$).

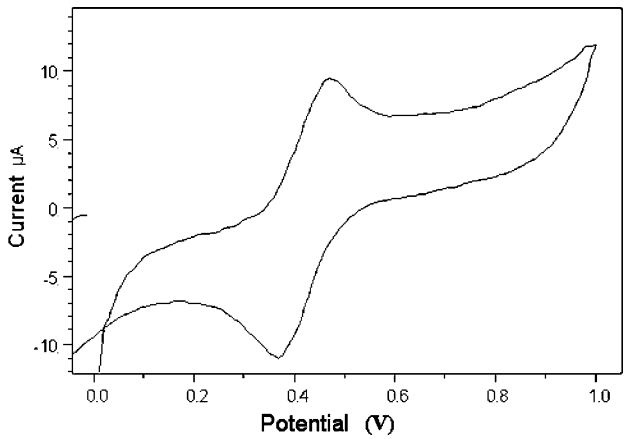


Fig. 11. Cyclic voltammetry of $[VO(L^3)]2H_2O$ in DMF in the presence of tetrabutylammonium hexafluorophosphate (0.1 M).

Therefore, we conclude that the oxidation potentials of the $[VOL^x]$ are affected by the size of the chelate ring of the ligands. However, upon oxidation, the dark red, brown or black compounds turned to an intense violet. Re-reduction yielded $[VOL^x]$ unchanged. The process could be repeated many times without any evidence of a chemical degradation. Cyclic voltammetry on $[VOL^x]nH_2O$ ($x = 1$–3) reveals a reduction potential value in the range expected for a five-coordinated mono oxovanadium species on the basis of other members in this series. The fact that the reduction is completely reversible indicates that the five-coordinate geometry is stable in both oxidation states, at least on the cyclic voltammetry time scale [22].

References

1. R.D. Archu and B. Wang, *Inorg. Chem.*, **29**, 39 (1990).
2. S. Chang, L. Jones, C.M. Henling and R.H. Grubbs, *Organometallics*, **17**, 3460 (1998).
3. S. Yamada, *Coord. Chem. Rev.*, **190**, 537 (1999).
4. B. De Clereq and F. Verpoort, *Macromolecules*, **35**, 8943 (2002).
5. A. Berkessel, M. Franvenkon, T. Schwenkreis and J. Steinmetz, *J. Mol. Catal. A: Chem.*, **117**, 39 (1997).
6. B. De De Clereq and F. Verpoort, *Adv. Synth. Catal.*, **34**, 639 (2002).
7. T. Opstal and F. Verpoort, *Synlett*, **6**, 935 (2002).
8. T. Opstal and F. Verpoort, *Angew Chem. Int. Ed.*, **42**, 2876 (2003).
9. B. De Clereq, F. Lefebvre and F. Verpoort, *Appl. Catal. A*, **247**, 345 (2003).
10. E.C. Niederhoffer, J.H. Timmons and A. Martell, *Chem. Rev.*, **84**, 137 (1984).
11. S. Zolezzi, E. Spodine and A. Decinti, *Polyhedron*, **21**, 55 (2002).
12. G.S. Patterson and R.H. Holm, *Bioinorg. Chem.*, **4**, 257 (1975).
13. G.H. Jeffery, J. Basset, J. Mendham and R.C. Denny, Vogel's Quantitative Chemical Analysis, 5th edn., Longmand Scientific and Technical Ltd., Essex (U.K.), 1989, p. 447.
14. A. Gölcü, M. Tümer, H. Demirelli and R.A. Wheatley, *Inorg. Chim. Acta*, **358**, 1705 (2005).
15. M. Tümer, *Synth. React. Inorg. Met. Org. Chem.*, **30**, 1139 (2000).
16. J.P. Costa and I. Cavaco, *Inorg. Chim. Acta*, **293**, 1 (1999).
17. M. Tümer, M. Deligönül, A. Gölcü, E. Akgün, M. Dolaz, H. Demirelli and M. Dığrak, *Transit. Met. Chem.*, **31**, 1 (2006).
18. M.S. El-Shahawi and A.F. Shoair, *Spectrochim. Acta Part A*, **60**, 121 (2004).
19. H. Demirelli, M. Tümer and A. Gölcü, *Bull. Chem. Soc. Jpn.*, **79**, 867 (2006).
20. B. Mondal, S. Chakraborty, P. Munshi, M.G. Walawalkar and G. K. Lahiri, *J. Chem. Soc., Dalton Trans.*, 2327 (2000).
21. M. Vilas Boas, C. Freire, B. de Castro, P.A. Christensen and A.R. Hillman, *Inorg. Chem.*, **36**, 4919 (1997).
22. J.A. Bonadies and C.J. Carrano, *J. Am. Chem. Soc.*, **108**, 4088 (1986).